Magmatic Eruptions and Iron Volatility in Deep-Sea Hydrothermal Fluids

Authors: Nicholas J. Pester, Kang Ding and William E. Seyfried, Jr.

This file contains the following **Supplementary Information** to the above manuscript:

Methods

Supplementary Figures DR1 - DR5

Supplementary Tables DR1 - DR6

Methods

Experimental Apparatus. Hydrothermal flow-through experiments were conducted at temperatures between 410 °C and 465 °C and pressures coincident with vapor-liquid/vapor-halite stability (220 – 400 bars) in NaCl dominated fluids (See Tables DR1-DR5 for details). The experiments were carried out in one of two similar pressure vessels constructed of different materials. Experiments 1 – 2 were conducted in a 316 stainless steel reactor (~110 cm^3), whereas experiments 3 – 5 utilized a newly designed Ti-alloy reactor (~165 cm^3). The experimental design is similar to that described in Foustoukos and Seyfried (2007b) with modifications as shown in Fig. DR2. For the Ti-alloy cell, all wetted accessory tubing/valves (including the pump head) were also constructed of Ti with exception of the output back-pressure regulating valve (316 ss), which operates at ambient temperature. A Ti-sheathed Type E (chromel-constantan) thermocouple was used for internal monitoring of the Ti-alloy cell. Uncertainties in pressure are constrained by the capability of the computer-controlled back-pressure regulator (± 0.5 bars under experimental conditions). This regulator is an air actuated (dome-loaded) valve connected to an ER3000™ electronic pressure controller (Tescom Industrial Controls). Vapor samples were collected after having passed through the back-pressure regulator to avoid any unnecessary decreases in pressure. This is important due to the *P-T* sensitivity of vapor chlorinity near critical conditions (Driesner and Heinrich, 2007). As such, liquid samples were only taken after

sufficient vapor sample had been acquired. Though operating at ambient temperature, there was still concern of metal contamination for the most dilute and acidic vapors due to contact with 316ss in the valve. However, a test using 0.05 N HCl (trace-metal grade) for similar residence times showed no meaningful metal contamination. In experiment 5 (Fig. 2), a computer controlled Ti metering valve was utilized to completely eliminate possible contamination, and in this case pressure variability was ± 2 – 3 bars.

Experimental Procedures. All starting solutions were prepared with deionized H_2O and ACS grade chloride salts. The bulk concentrations of Fe and Mn were set at levels consistent with those of natural hydrothermal fluids (1 – 10 mmol/kg). All solutions were titrated to a pH of ~ 3.0 with HCl prior to the addition of variably small amounts of formic acid. Upon heating, formic acid dissociates to equimolar amounts of CO_2 and H_2 and was used to assure the fH_2 in the cell was adequate to maintain redox sensitive Fe and Mn in the +2 state in solution. As such, measured H_2 concentrations in the single/vapor phases ranged 2.5 to 16 mmol/kg.

Throughout the experiments (and for 24 hours prior), all starting solutions were continuously purged with N_2 directly in the reservoir of the delivery pump to remove dissolved oxygen. The reactor (at ambient conditions) was also flushed with N_2, which was subsequently displaced by introduction of the source fluid. The cell was then heated to the desired temperature using the back-pressure regulator to maintain a setpoint ~20 bars above the fluid's critical point. High-temperature, single-phase flow was maintained until steady-state pH (25 °C) and dissolved gas concentrations (e.g. CO_2 and H_2, measured by gas chromatography) were achieved. Once achieved, a fluid sample was acquired. The chemical composition of this sample was compared to the reservoir solution to assure the chemical continuity of the system. The %RSD (2σ) between the unreacted start solution and the reacted (single-phase) solution was always less than 6%.

While flowing continuously, the two-phase region was typically approached by decreasing the set *P* on the back-pressure regulator along a given isotherm. At conditions in the two-phase region, flow rate of the source fluid was typically 0.1 – 0.3 cm^3/min, which was sufficient to achieve steady-state vapor chlorinity in good agreement with values predicted for equilibrium in the NaCl-H_2O system (Driesner and Heinrich, 2007). When a new *P-T* set-point was established, refractive index, pH (25 °C) and dissolved gas concentrations were monitored

until the new steady-state vapor composition was achieved. Usually only 15 – 20 minutes were required to achieve steady-state, however, fluid was allowed to flow for at least 45 minutes prior to acquiring vapor samples. Large samples of the highly dilute vapors (~10 – 20 g) were taken, which is a distinct advantage of the flow-through reactor configuration. Liquid-phase samples were acquired (after sufficient passage of fluid to rinse the sample line) by opening a flow-regulating valve (Ti). Samples for metal analysis were immediately acidified with trace-metal grade HCl.

Cl was analyzed by ion chromatography (2σ: ± 1%) and all cations (e.g. Na, Fe, Mn) were analyzed by inductively-coupled plasma optical emission spectroscopy (ICP-OES) with uncertainties of ± 4% (2σ). pH (25 °C) was measured using a Thermo-Ross electrode that was calibrated often during each sampling session. Charge balance (including pH) was confirmed to be within analytical uncertainty. Chemical data (and associated *P-T* conditions) from experiments 1-5 are reported in Tables DR1-DR5, where sample designations S, V and L are the starting fluid/single phase, vapors and liquids, respectively.

Fluid Chemistry from EPR, 9°50'N. Previously unpublished data from Bio 9, Bio 9' and P vent, incorporated into time-series data analyses, are given in Table DR6. Fluid samples were acquired in February 2004 and December 2007 – January, 2008 as part of *R/V Atlantis*/*DSV Alvin* expeditions AT-11-07 and AT-15-28 to the East Pacific Rise, respectively. Details regarding sample acquisition, analyses and analytical uncertainties are given in Pester et al. (2011). Samples were of high quality (i.e. minimal seawater was entrained during sampling) as exhibited by the minimum Mg concentrations (Mg_{min}). Data are reported as end-members derived by extrapolation to zero Mg to account for any seawater mixing (Von Damm, 2000). Reported errors are the greater of either the analytical uncertainty (2σ) or the 95% confidence interval of the extrapolation.

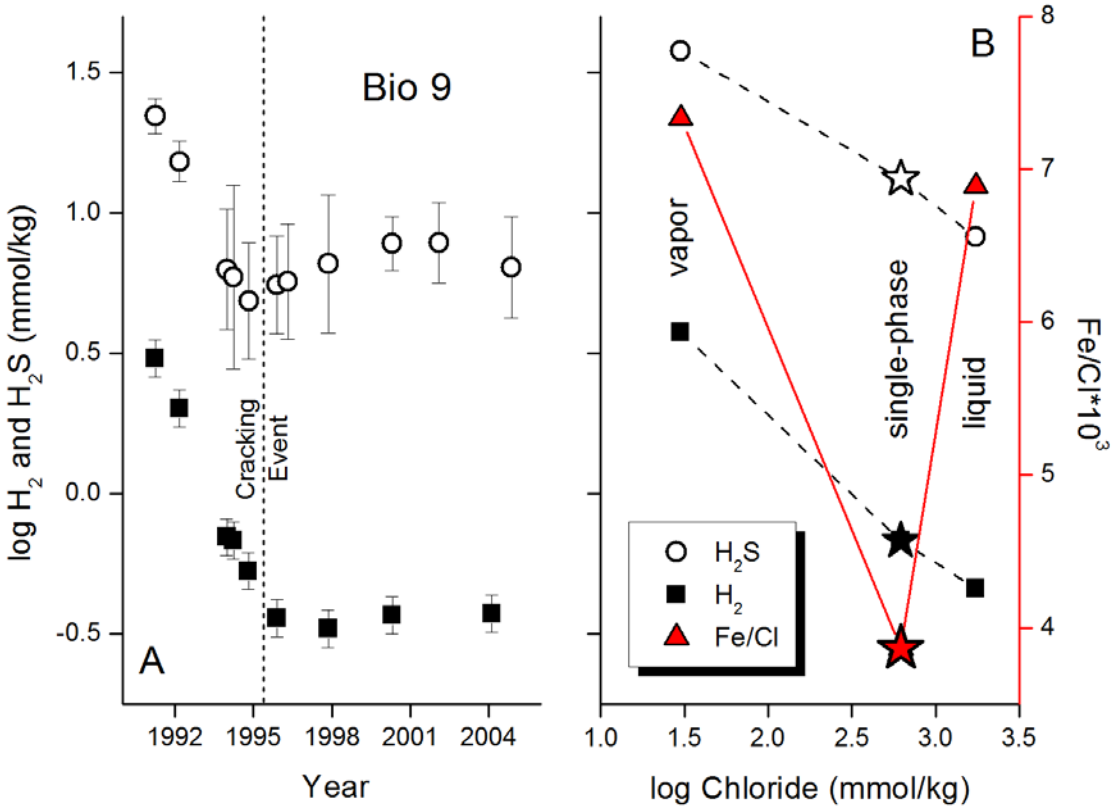

Supplementary Fig. DR1. Panel A: Time-series H_2 and H_2S concentrations in Bio 9 vent fluid (Von Damm, 2000, 2004; Von Damm and Lilley, 2004, Table DR6). The greatest concentrations are observed during the 1991 eruption. Values subsequently decline until steady-state is achieved (see also Fig. 1). Panel B: Experimental data from Foustoukos and Seyfried (2007a). A NaCl dominated fluid was initially equilibrated with PPM (redox buffer) and K-feldspar-muscovite-quartz (pH buffer) at near critical (single-phase) conditions (390 °C, 283 bars, star symbols), then subsequently re-equilibrated in the two-phase region (390 °C, 251 bars). The Fe/Cl ratio (red, right axis) of both the evolved vapor and liquid was twice that of the single phase. The vapor concentrations of H_2 and H_2S (left axis) also increased substantially (similar in magnitude to those observed for Bio 9 in Panel A) due to high solubility in low density vapors.

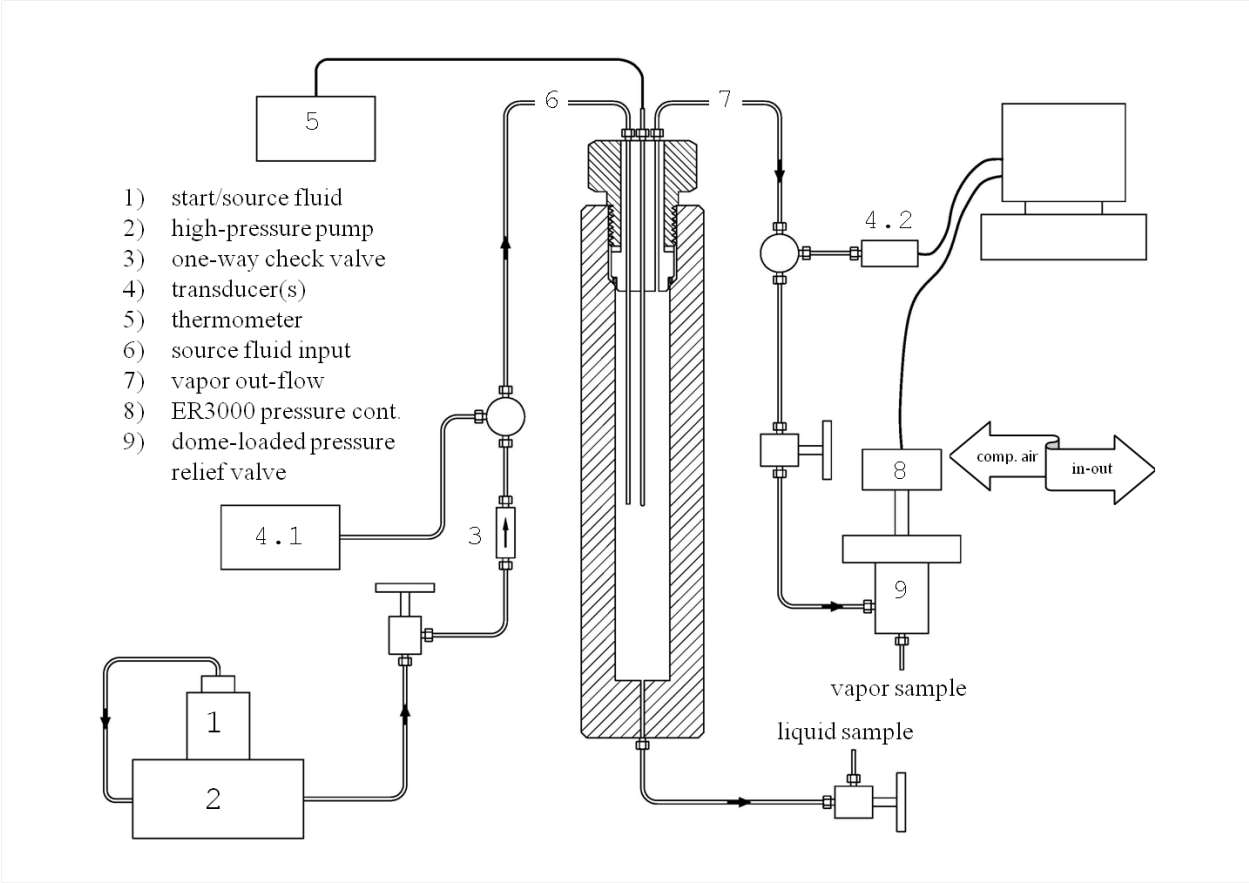

Supplementary Fig. DR2. Schematic diagram of the experimental flow system and Ti-alloy reaction cell used for the present study. The source fluid input line (6) terminates in the middle of the cell as does the internal (Ti-sheathed) thermocouple where temperature is logged by a digital thermometer (5). The external thermocouples and heating coils related to cell temperature control are not shown for clarity. Static pressure is maintained via computer interface between a transducer (4.2) and the ER3000™ unit (8) containing solenoid valves that rapidly inlet/exhaust compressed air to the dome of the pressure relief valve (9). Liquid samples were periodically retrieved using a manual valve. See Methods for further details.

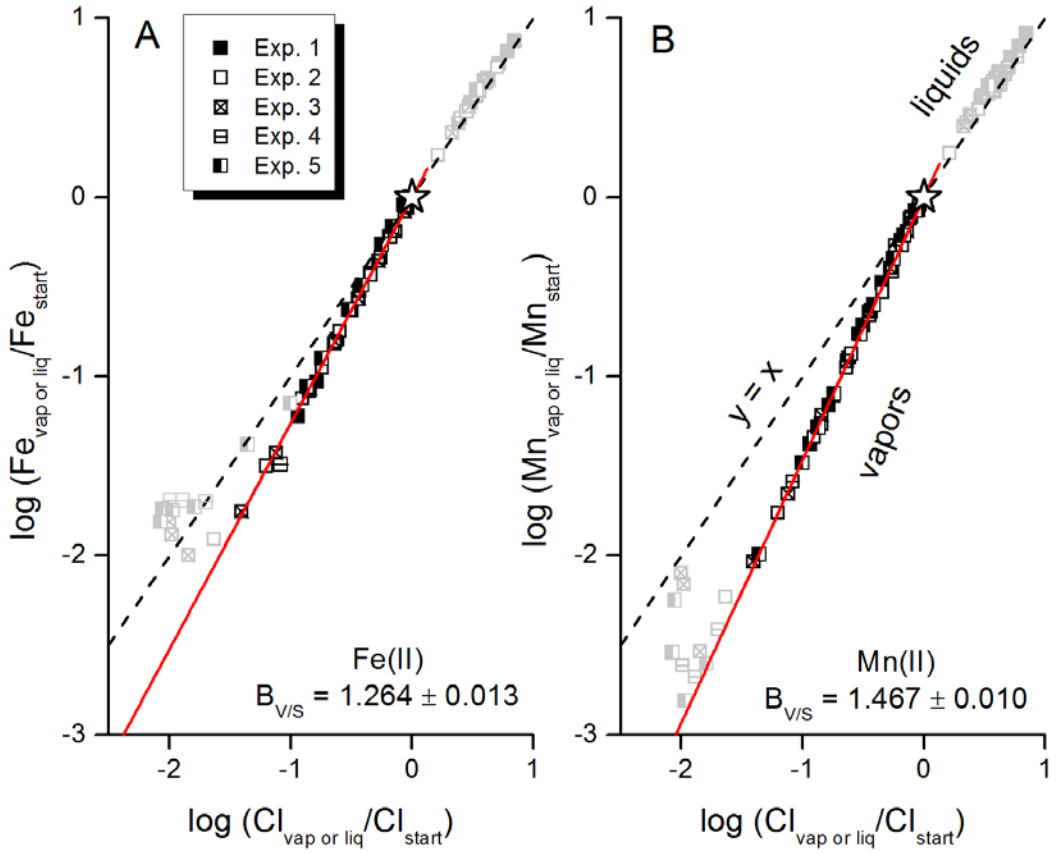

Supplementary Fig. DR3. Experimental data normalized for extraction of vapor-based partition coefficients ($B_{V/S}$, see below) for A) Fe(II) and B) Mn(II). See Tables DR1-DR5 for experimental conditions and fluid compositions. Vapor data showing no evidence of volatility are regressed (solid, red line) through the origin (and critical point, star symbol). Thus, the slope constitutes the partition coefficient $B_{V/S}$, where $\log (M_{vap}/M_{start}) = B_{V/S} * \log (Cl_{vap}/Cl_{start})$; and M_{vap}, Cl_{vap} and M_{start}, Cl_{start} are the metal and Cl concentrations in the vapor and starting solutions, respectively. The reported error of $B_{V/S}$ is the 95% confidence interval. This allows modeling the effects of phase separation on discrete (NaCl-dominated) solutions (i.e. $B_{V/S}$ value of Na is unity) following derivation of the relationships: log (Fe/Cl) = 0.264*log Cl and log (Mn/Cl) = 0.467*log Cl (as demonstrated in Fig. 2). Liquid-phase data and volatile vapor data not included in the regressions are shown in grey scale. The liquid phase data show little deviation from the line of unit slope (dashed, y = x).

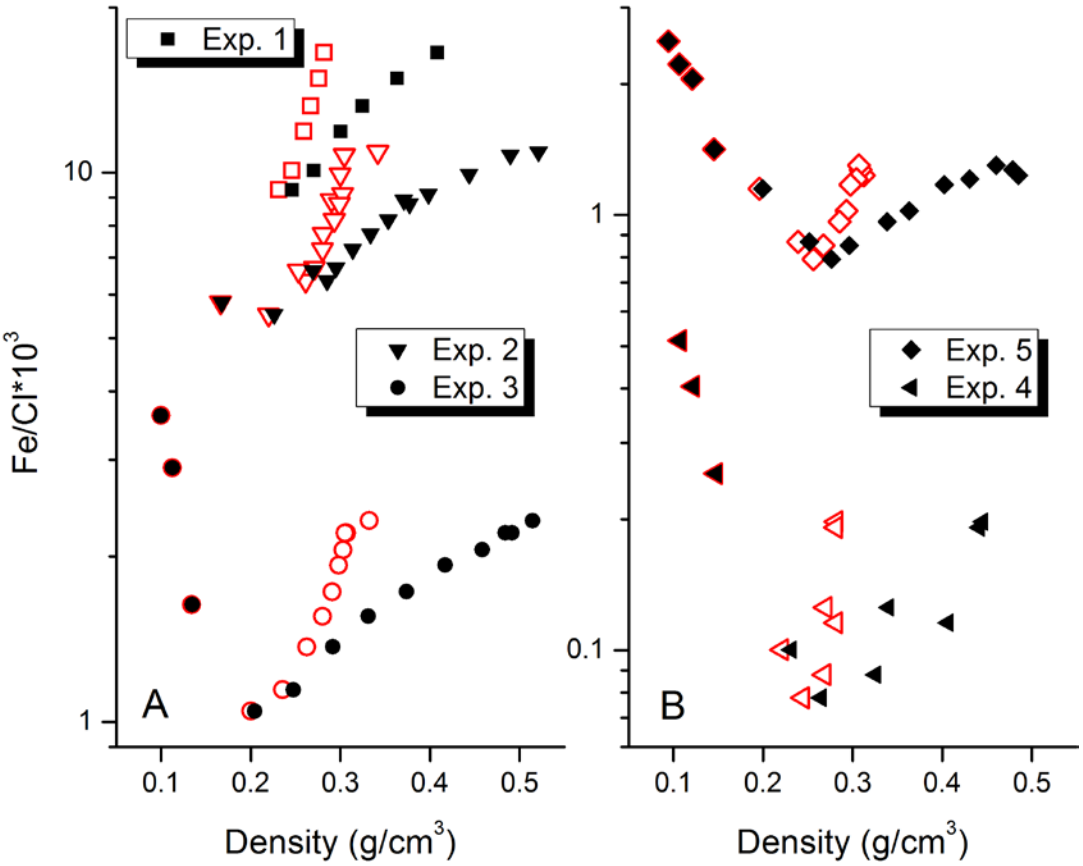

Supplementary Fig. DR4. Density vs. Fe/Cl of the vapors in A) experiments 1 – 3 and B) experiments 4 – 5 (note different y-axis scales). See Tables DR1-DR5 for additional experimental details. Filled symbols are the NaCl-H_2O densities at the measured *P*-*T*-x for the vapors (Driesner and Heinrich, 2007) whereas the open symbols are the density of pure H_2O at the same *P* and *T* (IAPWS-95). All experiments show the onset of Fe volatility coincides with where the vapors have become sufficiently dilute that the density is essentially equivalent to pure H_2O (~0.23 g/cm^3).

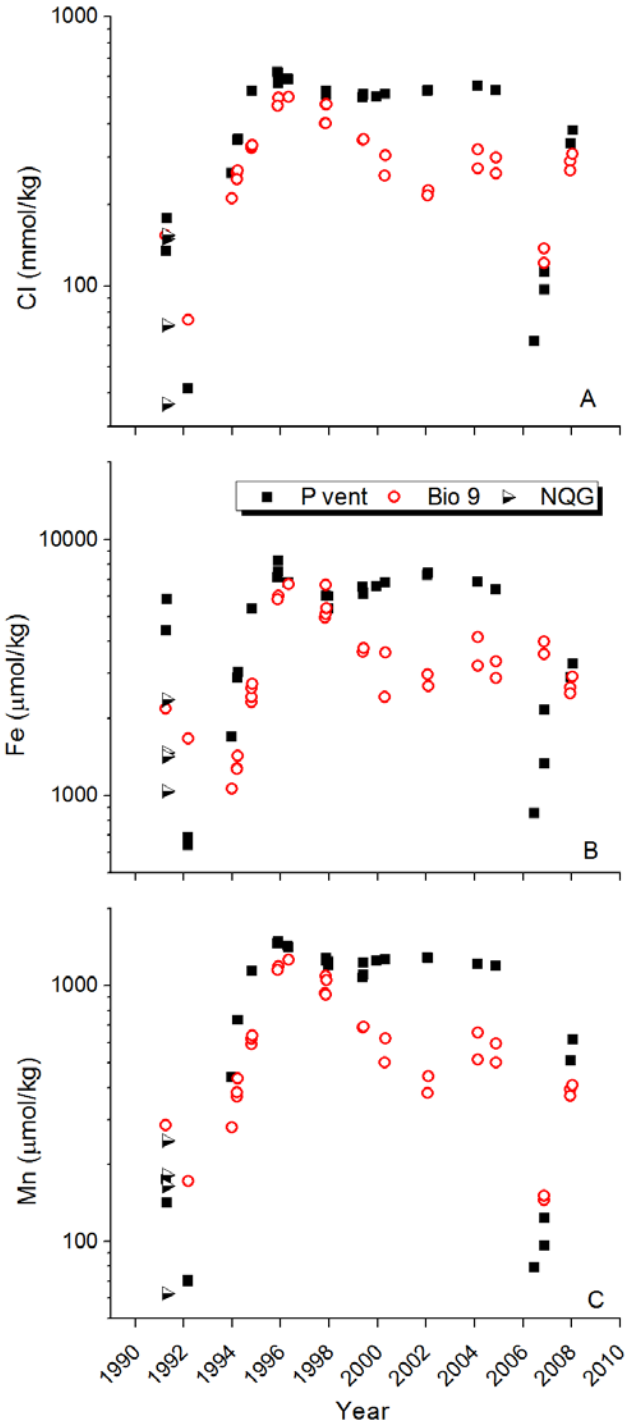

Supplementary Fig. DR5. Time-series fluid chemistry (Bryce et al., 2011; Fornari et al., 2012; Von Damm, 2000; 2004, Table DR6) from vent structures P vent and Bio 9 (plus N, Q and G vents in 1991) at EPR, 9°50'N including: A) dissolved Cl, B) dissolved Fe and C) dissolved Mn.

Table DR1.

Table DR1: Data from flow experiment 1

sample	T (°C)	P (bars)	Cl (mm)*	Fe (μm)	Mn (μm)	pH
1-S1	410	341.3	573	10343	1017	3.72
1-V1	410	309.1	376	6224	579	3.36
1-L1	410	309.1	1751	34945	3725	
1-V2	410	307.4	261	3871	337	3.28
1-L2	410	307.4	2433	47425	5049	
1-V3	410	304.9	182	2405	196	3.22
1-L3	410	304.9	2995	57440	6081	
1-V4	410	302.5	140	1665	130	3.17
1-L4	410	302.5	3536	67065	7013	
1-V5	410	298.3	95	958	70	3.20
1-L5	410	298.3	4039	76735	8255	
1-V6	410	293.5	66	616	43	3.13

* mm and μm are mmol and umol per kg solution, respectively

Table DR2.

Table DR2: Data from flow experiment 2

sample	T (°C)	P (bars)	Cl (mm)*	Fe (μm)	Mn (μm)	pH
2-S1	425	372.0	924	10090	1064	3.93
2-V1	425	356.0	832	8960	904	3.64
2-L1	425	356.0	1507	17408	1873	3.98
2-V2	425	353.9	612	6083	572	3.45
2-L2	425	353.9	2327	27830	2988	4.12
2-V3	425	349.8	340	3032	249	3.32
2-L3	425	349.8	3147	37448	3992	4.56
2-V4	425	345.6	234	1805	142	3.25
2-L4	425	345.6	3732	43498	4643	4.73
2-V5	425	336.4	132	836	58	3.19
2-L5	425	336.4	4645	53343	5660	4.55
2-V6	440	395.0	510	4654	410	3.33
2-L6	440	395.0	2603	30365	3308	4.19
2-V7	440	392.7	422	3704	314	3.24
2-L7	440	392.7	3124	36840	4028	4.26
2-V8	440	389.3	333	2735	232	3.26
2-L8	440	389.3	3819	44783	5235	4.57
2-V9	440	380.8	212	1533	119	3.16
2-V10	439	375.2	167	1121	82	3.12
2-V11	439	364.6	114	759	49	3.08
2-V12	439	344.5	58	320	18	3.01
2-V13	439	304.3	22	125	6.2	2.80

* mm and μm are mmol and umol per kg solution, respectively

Table DR3.

Table DR3: Data from flow experiment 3

sample	T (°C)	P (bars)	Cl (mm)*	Fe (µm)	Mn (µm)	pH, 25C
3-S1	426	370.5	910	2114	1907	2.84
3-V1	425	356.6	839	1851	1735	2.75
3-L1	425	356.6	1948	4849	4746	4.20
3-V2	424	354.5	795	1756	1617	2.77
3-L2	424	354.5	2189	5479	5490	4.08
3-V3	424	351.8	662	1361	1231	2.76
3-L3	424	351.8	2686	6767	6804	4.40
3-V4	423	346.9	481	928	770	2.79
3-L4	423	346.9	3269	8224	8101	4.60
3-V5	422	342.1	332	573	441	2.76
3-L5	422	342.1	3565	9434	8786	5.24
3-V6	421	335.8	212	330	232	2.74
3-L6	421	335.8	3901	9633	9295	5.12
3-V7	420	327.2	131	180	116	2.73
3-V8	420	315.0	69	79	42	2.72
3-V9	420	297.7	36	37	18	2.69
3-V10	464	297.7	13	21	5.6	2.57
3-V11	465	267.9	9.5	28	13	2.43
3-V12	466	247.4	9.1	33	15	2.30

* mm and µm are mmol and umol per kg solution, respectively

Table DR4.

Table DR4: Data from flow experiment 4

sample	T (°C)	P (bars)	Cl (mm)*	Fe (µm)	Mn (µm)	pH
4-S1	410	320	634	164	2020	
4-V1	410	308.3	501	99	1576	
4-L1	410	308.3	2328	892	8962	
4-V2	410	308.2	488	93	1528	
4-L2	410	308.2	1956	652	7536	
4-V3	410	308.2	371	43	1084	
4-L3	410	308.2	1422	574	5266	
4-V4	410	305.3	224	28	464	
4-V5	410	304.9	183	16	350	
4-L5.1	410	304.9	3103	672	10605	
4-L5.2	410	304.9	2930	576	10134	
4-L5.3	410	304.9	2761	517	9301	
4-L5.4	410	304.9	2382	460	8002	
4-V6	411	299.5	84	6.5	106	
4-L6.1	411	299.5	3738	601	12263	
4-L6.2	411	299.5	2966	247	9827	
4-L6.3	411	299.5	2694	216	8582	
4-L6.4	411	299.5	2449	172	7795	
4-V7	409	288.8	52.64	5.3	52	3.22
4-V8	409	250.0	12.71	3.2	7.8	3.11
4-V9	431	250.0	8.20	3.3	4.3	2.92
4-V10	453	250.0	6.45	3.3	4.9	2.74

* mm and µm are mmol and umol per kg solution, respectively

Table DR5.

Table DR5: Data from flow experiment 5

sample	T (°C)	P (bars)	Cl (mm)*	Fe (µm)	Mn (µm)	pH
5-S2	440	400	953	1175	984	2.78
5-V1	440	398	930	1180	955	2.72
5-V2	439	394	816	1062	823	2.70
5-V3	439	392	661	798	602	2.67
5-B4	438	390	3258	4656	4074	3.84
5-V5	438	387	541	635	444	2.67
5-V6	438	384	370	378	247	2.66
5-V7	438	379	287	277	168	2.65
5-V8	437	368	173	147	79	2.63
5-V9	437	361	130	103	51	2.62
5-V10	437	351	95	82	32	2.63
5-V11	436	323	42	49	10.0	2.61
5-V12	437	282	15	22	2.5	2.55
5-V13	437	255	10.2	21	1.51	2.52
5-V14	438	237	8.1	18	2.8	2.41
5-V15	439	220	8.5	21	5.5	2.19

* mm and µm are mmol and umol per kg solution, respectively

Table DR6.

Table DR6: Selected end-member vent fluid chemistry from EPR, 9°50'N[A]

Vent	T_{exit} (°C)	# samples	Mg_{min} (mm)	Cl (mm)*	Fe (µm)	Mn (µm)	Si (mm)	H_2 (µmol/L)
February, 2004								
Bio9	366	3	1.5	321 ± 4	4162 ± 391	655 ± 28	10.2 ± 1.2	373 ± 37
Bio9'	383	3	3.4	273 ± 3	3224 ± 499	512 ± 44	9.9 ± 1.0	na
P-vent	364	6	1.3	552 ± 6	6847 ± 274	1216 ± 49	14.7 ± 0.6	183 ± 18
December, 2007 - January, 2008								
Bio 9	330	2	1.9	309 ± 11	2912 ± 116	407 ± 16	10.0 ± 0.4	1060 ± 106
P vent	374	3	2.0	379 ± 7	3262 ± 130	616 ± 25	11.8 ± 0.5	525 ± 53

A) see methods for further details * mm and µm are mmol and umol per kg solution, respectively

References

Bryce, J., Prado, F., and Von Damm, K., 2011, Marine Geoscience Data System, www.marine-geo.org, doi:10.1594/IEDA/100031.

Driesner, T., and Heinrich, C. A., 2007, The system H_2O-NaCl. Part I: Correlation formulae for phase relations in temperature-pressure-composition space from 0 to 1000°C, 0 to 5000 bar, and 0 to 1 X_{NaCl}: Geochimica et Cosmochimica Acta, v. 71, p. 4880-4901.

Fornari, D. J., Von Damm, K. L., Bryce, J. G., Cowen, J. P., Ferrini, V., Fundis, A., Lilley, M. D., Luther III, G. W., Mullineaux, L. S., Perfit, M. R., Meana-Prado, M. F., Rubin, K. H., Seyfried, W. E., Jr., Shank, T. M., Soule, S. A., Tolstoy, M., and White, S. M., 2012, The East Pacific Rise between 9°N and 10°N: Twenty-five years of integrated, multidisciplinary oceanic spreading center studies: Oceanography, v. 25, p. 18-43.

Foustoukos, D. I., and Seyfried, W. E., Jr., 2007a, Fluid phase separation processes in submarine hydrothermal systems, *in* Liebscher, A., and Heinrich, C. A., eds., Fluid–Fluid Interactions, Rev. Mineral. Geochem. 65: Chantilly, VA., MSA, p. 213-239.

Foustoukos, D. I., and Seyfried, W. E., Jr., 2007b, Trace element partitioning between vapor, brine and halite under extreme phase separation conditions Geochimica et Cosmochimica Acta, v. 71, p. 2056-2071.

Pester, N. J., Rough, M., Ding, K., and Seyfried, W. E., Jr., 2011, A new Fe/Mn geothermometer for hydrothermal systems: Implications for high-salinity fluids at 13°N on the East Pacific Rise: Geochimica et Cosmochimica Acta, v. 75, p. 7881-7892.

Von Damm, K. L., 2000, Chemistry of hydrothermal vent fluids from 9°-10°N, East Pacific Rise: "Time zero," the immediate posteruptive period: Journal of Geophysical Research, v. 105, p. 11203-11222.

Von Damm, K. L., 2004, Evolution of the hydrothermal system at East Pacific Rise 9º50´N: Geochemical evidence for changes in the upper oceanic crust, *in* German, C. R., Lin, J., and Parson, L. M., eds., Mid-Ocean Ridges: Hydrothermal Interactions Between the Lithosphere and Oceans, Geophys. Monogr. Ser., 148: Washington, D.C., AGU, p. 285-305.

Von Damm, K. L., and Lilley, M. D., 2004, Diffuse flow hydrothermal fluids from 9°50'N East Pacific Rise: Origin, evolution and biogeochemical controls, *in* Wilcock, W. S., Cary, C., De Long, E., Kelley, D., and Barross, J., eds., The Subseafloor Biosphere at Mid-Ocean Ridges, Geophys. Monogr. Ser., 144: Washington, D.C., AGU, p. 245-268.